Chemical Science

ROYAL SOCIETY OF CHEMISTRY

EDGE ARTICLE

View Article Online
View Journal | View Issue

Check for updates

Cite this: *Chem. Sci.*, 2023, **14**, 6564

All publication charges for this article have been paid for by the Royal Society of Chemistry

Monoarsine-protected icosahedral cluster $[Au_{13}(AsPh_3)_8Cl_4]^+$: comparative studies on ligand effect and surface reactivity with its stibine analogue†

Jiu-Hong Yu,[a] Zhi-Rui Yuan,[a] Jing Xu,[a] Jin-Gui Wang,[a] Mohammad Azam,[c] Tian-Duo Li,[a] Ying-Zhou Li *[a] and Di Sun *[b]

Ligand shells of gold nanoclusters play important roles in regulating their molecular and electronic structures. However, the similar but distinct impacts of the homologous analogues of the protecting ligands remain elusive. The C_{2v} symmetric monoarsine-protected cluster $[Au_{13}(AsPh_3)_8Cl_4]^+$ (**$Au_{13}As_8$**) was facilely prepared by direct reduction of $(Ph_3As)AuCl$ with $NaBH_4$. This cluster is isostructural with its previously reported stibine analogue $[Au_{13}(SbPh_3)_8Cl_4]^+$ (**$Au_{13}Sb_8$**), enabling a comparative study between them. **$Au_{13}As_8$** exhibits a blue-shifted electronic absorption band, and this is probably related to the stronger π-back donation interactions between the Au_{13} core and $AsPh_3$ ligands, which destabilize its superatomic 1P and 1D orbitals. In comparison to the thermodynamically less stable **$Au_{13}Sb_8$**, **$Au_{13}As_8$** achieves a better trade-off between catalytic stability and activity, as demonstrated by its excellent catalytic performance towards the aldehyde–alkyne–amine (A^3) coupling reaction. Moreover, the ligand exchange reactions between **$Au_{13}As_8$** with phosphines, as exemplified by PPh_3 and $Ph_2P(CH_2)_2PPh_2$, suggest that **$Au_{13}As_8$** may be a good precursor cluster for further cluster preparation through the "cluster-to-cluster" route.

Received 12th March 2023
Accepted 28th May 2023

DOI: 10.1039/d3sc01311a

rsc.li/chemical-science

Open Access Article. Published on 29 May 2023. Downloaded on 2/15/2026 12:58:01 AM.
This article is licensed under a Creative Commons Attribution-NonCommercial 3.0 Unported Licence.

Introduction

The icosahedral Au_{13} core is considered a fundamental building block which is commonly observed as the metal core in various structurally well-defined Au nanoclusters.[1–17] It was theoretically found that the electronic structures of the Au_{13} unit might dictate the physicochemical properties of its assembled clusters.[18–21] It is therefore of importance to study the influencing factors in depth on the geometric and electronic structures of the individual icosahedral Au_{13} clusters. In this context, the past 15 years have first witnessed a renewed interest in the typical phosphine-protected Au_{13} clusters involving development of new synthetic routes (*e.g.*, HCl-induced convergence),[6,7,22,23] exploration of formation mechanisms,[24,25] tuning of electronic properties (*e.g.*, by heterometal doping[26–29]), and optical properties (*e.g.*, NIR emission[6,7,30] and chiroptical activity[31–33]), as well as further expansion of their potential applications (*e.g.*, photodynamic catalysis and nano-electronic devices).[34,35] More recently, comparative studies on several new types of Au_{13} analogues protected by other pnictines (*e.g.*, functionalized diphosphine,[36] phosphinous acid,[37] diarsine,[38] and monostibine[39–41]) or mimics of pnictine (*N*-heterocyclic carbenes)[42–47] have also been extensively made both experimentally and theoretically.

The large number of studies on icosahedral Au_{13} clusters showed that the stereoelectronic factors of the pnictine/NHC ligands have a non-negligible influence on their electronic structures.[14,48–54] These ligand-based influencing factors, however, are often intertwined with other factors such as the core geometry and cluster charge state. For example, in 2021, the Konishi group synthesized a pair of dipnictine-protected clusters $[Au_{13}(dppe)_5Cl_2]^{3+}$ (dppe = $Ph_2P(CH_2)_2PPh_2$) and $[Au_{13}(dpap)_5Cl_2]^{3+}$ (dpap = $Ph_2As(CH_2)_3AsPh_2$), and demonstrated that the Au_{13} core geometry (deformation), rather than the coordinating P or As atoms, has a more pronounced effect on their absorption and photoluminescence properties.[38] In this sense, it is necessary to employ Au_{13} cluster analogues, with essentially the same metal cores and ligand arrangements, as the comparable cases for better understanding the pnictine

[a]*School of Chemistry and Chemical Engineering, Qilu University of Technology (Shandong Academy of Sciences), Ji'nan, 250353, P. R. China. E-mail: liyz@qlu.edu.cn*
[b]*School of Chemistry and Chemical Engineering, State Key Laboratory of Crystal Materials, Shandong University, Ji'nan, 250100, P. R. China. E-mail: dsun@sdu.edu.cn*
[c]*Department of Chemistry, College of Science, King Saud University, P. O. Box 2455, Riyadh 11451, Saudi Arabia*

† Electronic supplementary information (ESI) available: Experimental procedures, computational and crystallographic details, and spectroscopic characterization including IR, ESI-MS, UV-vis, and NMR. CCDC 2244318 and 2244690. For ESI and crystallographic data in CIF or other electronic format see DOI: https://doi.org/10.1039/d3sc01311a

© 2023 The Author(s). Published by the Royal Society of Chemistry

Open Access Article. Published on 29 May 2023. Downloaded on 2/15/2026 12:58:01 AM. This article is licensed under a Creative Commons Attribution-NonCommercial 3.0 Unported Licence.

ligand effect. The monopnictine-protected Au_{13} clusters may serve as good candidates for this purpose since the monopnictines are usually more fluxional in the coordination sphere, and the Au_{13} core geometry is expected to be less affected by the ligands due to the absence of (possibly) strained Au–L′–Au staple/bridge moieties (L′ = bridging ligands). Unfortunately, few has been done with the monopnictine-protected Au_{13} clusters, largely due to the lack of comparable analogue clusters with known crystal structures.

To our knowledge, only four monophosphine-protected Au_{13} clusters have been reported, *i.e.*, $[Au_{13}(PMe_2Ph)_{10}Cl_2]^{3+}$, $[Au_{13}(PMePh_2)_8Cl_4]^+$, $[Au_{13}(POct_3)_8Cl_4]^+$ ($POct_3$ = trioctylphosphine) and $[Au_{13}(L)_8Cl_4]^+$ (L = $P(CH_2CH_2CO_2CH_3)_3$), and the last of these could further convert to Au_{25} nanoclusters by reacting with thiols.[2,3,7,16] In contrast, much less is known about their heavier analogues. In 2018, we reported the monostibine-protected Au_{13} cluster $[Au_{13}(SbPh_3)_8Cl_4]^+$ (**$Au_{13}Sb_8$**),[39] which was found more amenable to ligand exchange and also more catalytically active than PPh_3-protected Au_{11} clusters.[40,41] Systematic studies on monoarsine-protected Au_{13} clusters have lagged behind, despite the structurally similar cluster $[Au_{16}(AsPh_3)_8Cl_6]$ published long ago.[55] We are thus intrigued by further synthesis of the $AsPh_3$-protected Au_{13} clusters, so as to better understand the heavier pnictine ligand effect on their structures and reactivities by comparative studies with their heavier analogue **$Au_{13}Sb_8$**.

Herein, we present the synthesis, characterization and reactivity of the monoarsine-protected cluster $[Au_{13}(AsPh_3)_8Cl_4]^+$ (**$Au_{13}As_8$**) which is isostructural with its heavier analogue **$Au_{13}Sb_8$**, in terms of the core geometry and ligand arrangement. Comparative studies between them revealed that the blue-shift electronic absorption band of **$Au_{13}As_8$** is probably related to the stronger π-back donation interactions between the Au_{13} core and $AsPh_3$ ligands, which destabilize its superatomic 1P and 1D orbitals. Moreover, **$Au_{13}As_8$** is thermodynamically more stable than its stibine counterparts due to the moderate Au–As coordination bond strength, but its surface arsine ligands are kinetically more labile than phosphines. The unique characteristic of **$Au_{13}As_8$** enables a better trade-off between its catalytic stability and activity, and also makes it an ideal candidate for the precursor cluster in the preparation of other clusters *via* the "cluster-to-cluster" strategy.

Results and discussion

Synthesis and characterization

Briefly, **$Au_{13}As_8$** was prepared by direct reduction of $(Ph_3As)AuCl$ with 0.5 equivalent of $NaBH_4$ in dichloromethane (DCM)–ethanol mixed solvent (Scheme 1). The identity of the precursor

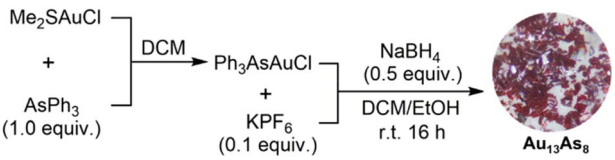

Scheme 1 Synthetic route to $Au_{13}As_8$.

$(Ph_3As)AuCl$ was first confirmed prior to reduction (Fig. S1†). After reduction, the crude **$Au_{13}As_8$** could be easily precipitated from its DCM solution by addition of hexane and is proved to be fairly pure by comparison of its IR spectrum with that of the purer crystalline **$Au_{13}As_8$**, which was obtained from its DCM–hexane solution by slow evaporation. In addition, the primary byproduct in this reaction, mainly found in the supernatant separated in the step of using hexane to precipitate the crude **$Au_{13}As_8$**, was identified as $(Ph_3As)_3AuCl$ by X-ray diffraction analysis (Fig. S2†). This finding provides strong evidence that even minor alterations to the reaction conditions, such as the type of solvent or quantity of reducing agent used, can have a considerable impact on the structure of the resulting product.[55]

Crystallographic data showed that **$Au_{13}As_8$** crystallized in a monoclinic lattice with the $P2_1/n$ space group (Table S1†). Two crystallographically independent molecules of **$Au_{13}As_8$**, with almost the same bond parameters, are present in the unit cell (Fig. S3†). Each comprises an icosahedral Au_{13} core, eight $AsPh_3$ ligands and four Cl^- ligands (Fig. 1). As is the case with its heavier analogue **$Au_{13}Sb_8$**,[39] the ligands in **$Au_{13}As_8$** also arranged in an approximate C_{2v} symmetry. The radial Au–Au bond lengths range from 2.726(2) Å to 2.810(2) Å (2.757(2) Å on average), while the peripheral ones are in the range of 2.808(2)–2.985(2) Å (2.900(2) Å on average). The Au–Cl bond lengths fall in the range of 2.31(1)–2.37(1) Å. The Au–As bond lengths range from 2.392(4) Å to 2.414(6) Å, which is longer than that in its precursor complex $(Ph_3As)AuCl$ (2.334(1) Å). As expected, these Au–Au and Au–Cl bond lengths in **$Au_{13}As_8$** are also quite close to the corresponding ones in **$Au_{13}Sb_8$** (Table S2†).

The mass spectrum of **$Au_{13}As_8$** shows a major peak at m/z = 5151.7672, attributed to the molecular ion $[Au_{13}(AsPh_3)_8Cl_4]^+$ (calcd = 5151.7738), which matches well with its calculated one; the isotopic interval of 1.0 amu support its +1 charge (Fig. 2). Besides, the ^{31}P NMR of the product shows a heptet resonance ascribable to PF_6^- (Fig. S4†), and its IR spectrum also shows the characteristic absorptions of PF_6^- at 839 and 557 cm^{-1} (Fig. S5†). All these indicate that **$Au_{13}As_8$** bears +1 charge, and the counterion is most probably PF_6^-, though it fails to be appropriately located crystallographically, probably due to its severe disorder.

The ^1H NMR spectrum of **$Au_{13}As_8$** shows three doublet resonances in the lower magnetic field (*ca.* 7.10–7.50 ppm)

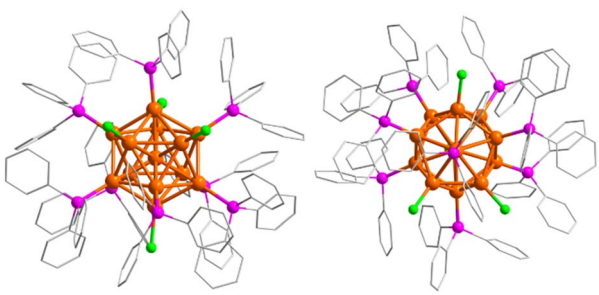

Fig. 1 Crystal structure of $Au_{13}As_8$ with all hydrogen atoms omitted (left: side view; right: top view). Au: orange, As: magenta, Cl: green, C: grey.

Open Access Article. Published on 29 May 2023. Downloaded on 2/15/2026 12:58:01 AM. This article is licensed under a Creative Commons Attribution-NonCommercial 3.0 Unported Licence.

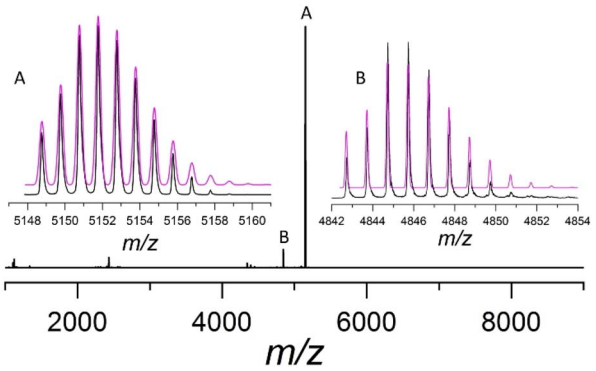

Fig. 2 ESI-MS(+) spectrum of $Au_{13}As_8$ in CH_2Cl_2. Inset: the experimental (black trace) and calculated (magenta trace) isotopic patterns of the $Au_{13}As_8$ ion (A) $[Au_{13}(AsPh_3)_8Cl_4]^+$ and its fragment ion (B) $[Au_{13}(AsPh_3)_7Cl_4]^+$.

region in an integration ratio of 1 : 2 : 1, and with a pattern quite akin to that of $Au_{13}Sb_8$ (Fig. S6†). This suggests the presence of three types of chemically non-equivalent $AsPh_3$ ligands, which is consistent with its solid-state structure; this also further confirms that the icosahedral Au_{13} clusters are stereochemically more rigid than the phosphine-protected Au_{11} clusters.[56,57]

Theoretical calculations

Since the $Au_{13}As_8$ and $Au_{13}Sb_8$ are isostructural either in the solid state or in solution, they constitute a good comparable pair for comparatively studying the heavier pnictine ligand effect on their structures and reactivities. As shown in Fig. 3, the experimental electronic absorptions for $Au_{13}As_8$ appear at 346 and 439 nm, which are blue-shifted by 6 and 15 nm, respectively, as compared to those for $Au_{13}Sb_8$ at 352 and 454 nm. Interestingly, the absorptions for the previously reported monophosphine-protected Au_{13} clusters are further blue-shifted (Fig. S7†).[2,3,7] Given the more similar structures of $Au_{13}As_8$ and $Au_{13}Sb_8$, TD-DFT calculations for them were performed at the same level of theory, to reveal the stereoelectronic

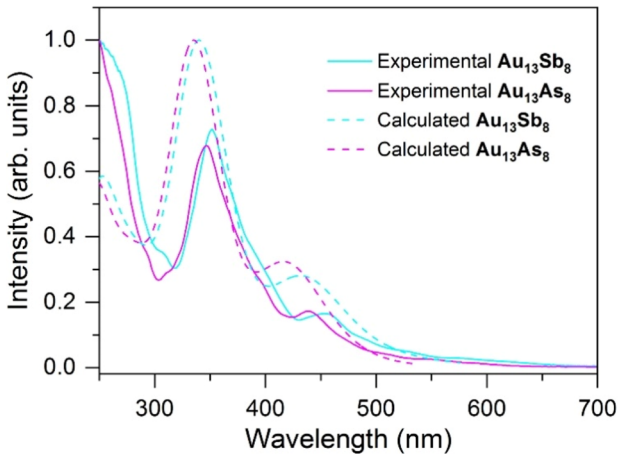

Fig. 3 Experimental (solid lines) and TD-DFT calculated (dash lines) UV-vis spectra for $Au_{13}As_8$ (magenta traces) and $Au_{13}Sb_8$ (cyan traces) in CH_2Cl_2.

influences of the pnictine ligands on the absorptions; the metal cores in both after structure relaxation are more of C_{2v} symmetry, probably transferred from the ligand shells and reflected by the continuous symmetry measure (CSM) value of 0.00 for both.[58] The optimized Au–Au bond lengths in $Au_{13}As_8$ are also slightly longer than those in $Au_{13}Sb_8$ (Table S3†), which is consistent with the crystallographic data. The calculated UV-vis spectra of them are well matched with their respective experimental ones, despite a small blue-shift, probably due to the overestimation of the excitation energies for the functional employed (Fig. S8 and S9†). Thus, the calculated peaks at 335 and 417 nm for $Au_{13}As_8$ (340 and 435 nm for $Au_{13}Sb_8$) should correspond to its experimental ones at 346 and 439 nm (352 and 454 nm for $Au_{13}Sb_8$), respectively.

$Au_{13}As_8$ and $Au_{13}Sb_8$ possess a similar electronic structure, with a HOMO–LUMO gap of 3.32 and 3.09 eV, respectively. The HOMO, HOMO − 1 and HOMO − 2 orbitals are typical of 1P superatomic orbitals while LUMO through LUMO + 4 show 1D characteristics (Tables S4 and S5†). The long-wavelength absorptions (417 nm for $Au_{13}As_8$ and 435 nm for $Au_{13}Sb_8$) are mainly ascribable to metal-to-metal charge transfer (MMCT) transitions from 1P to 1D shell, while the shorter-wavelength absorptions (335 nm for $Au_{13}As_8$ and 340 nm for $Au_{13}Sb_8$) are mainly attributed to ligand-to-metal charge transfer (LMCT) transitions to 1P orbitals from higher-lying occupied orbitals (HOMO − 3 to *ca.* HOMO − 10). In addition, the absorptions below 300 nm for both result from the even higher-energy transitions, such as HOMO − n (n > 15) to 1D, or HOMO − n (n < 5) to LUMO + n (n > 10); the phenyl rings in the ligands contributed significantly to HOMO − n (n > 15) orbitals with energy lower than −8.2 eV, and LUMO + n (n > 10) orbitals with energy higher than −2.2 eV (Fig. 4a, b and Tables S6, S7†).

As shown in Fig. 4c, on average, the 1P orbitals of $Au_{13}As_8$ comprise Au 5d/6sp orbitals (*ca.* 64%), As 4sp orbitals (*ca.* 13%), Cl 3sp orbitals (*ca.* 9%) and C 2sp orbitals (*ca.* 14%). The 1D orbitals are also mainly composed of Au atomic orbitals (Au : As : Cl : C = 72 : 13 : 3 : 12). The proportions of Au and As in orbitals from HOMO − 3 to HOMO − 10 decreased to a certain extent (48% for Au and 7% for As), but those of Cl and phenyl rings increased (21% for Cl and 24% for C). This means that, for a given type of cluster $[Au_{13}(ER_3)_8Cl_4]^+$ (E = pnictogen), the R substituent of ER_3 and the inorganic Cl^- may less affect the longer-wavelength absorptions resulting from 1P to 1D transitions, due to their less contributions to 1P/D orbitals; in other words, the shorter-wavelength absorptions are more susceptible to the stereoelectronic property of the ER_3 ligand. Consistent with this are the experimental UV-vis spectra of $[Au_{13}(L)_8Cl_4]^+$ (L = PPh_2Me; $P(CH_2CH_2CO_2CH_3)_3$),[3,16] which show almost the same absorption peaks at 432 nm in the lower-energy region but obviously different peaks at 342 nm and 333 nm, respectively, in the higher-energy region (Fig. S7†).

The orbital composition pattern of $Au_{13}Sb_8$ is akin to that of $Au_{13}As_8$. The 1P orbitals are composed of Au 5d/6sp (*ca.* 63%), Sb 5sp (*ca.* 13%), Cl 3sp (*ca.* 13%) and C 2sp (*ca.* 12%) orbitals. The 1D orbitals also mainly comprise Au atomic orbitals (Au : Sb : Cl : C = 67 : 17 : 4 : 11). The proportions of Au and As from HOMO − 3 to HOMO − 10 also decreased (44% for Au and 6%

© 2023 The Author(s). Published by the Royal Society of Chemistry

Open Access Article. Published on 29 May 2023. Downloaded on 2/15/2026 12:58:01 AM.
This article is licensed under a Creative Commons Attribution-NonCommercial 3.0 Unported Licence.

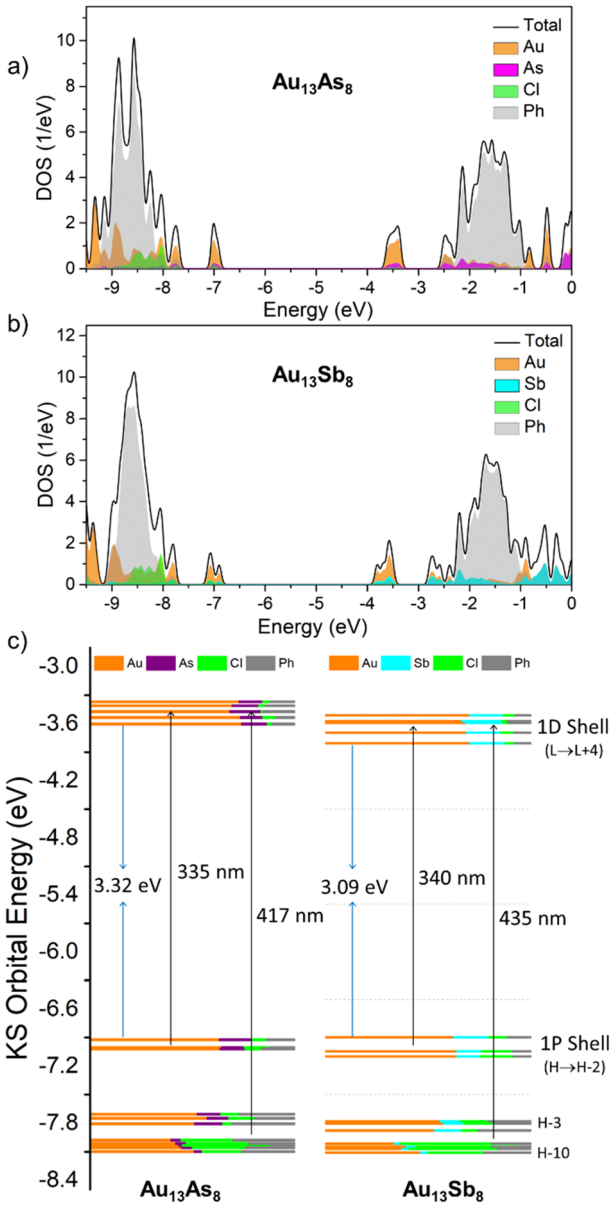

Fig. 4 Total density-of-states (TDOS) and partial density-of-states (PDOS) spectra of (a) $Au_{13}As_8$, (b) $Au_{13}Sb_8$, and (c) their selected Kohn–Sham molecular orbitals showing the populations of atomic orbitals.

for Sb), but those of Cl and phenyl rings increased (29% for Cl and 20% for C). In comparison, the superatomic 1P, 1D and the higher-lying occupied orbitals (*e.g.* HOMO − 3 to HOMO − 10) in **$Au_{13}As_8$** all up-shifted relative to their counterparts in **$Au_{13}Sb_8$**, except for the HOMO in **$Au_{13}As_8$**, which is marginally lower in energy by 0.025 eV than that in **$Au_{13}Sb_8$**.

Previous studies with thiol/alkynyl-protected Au_{25} clusters based on the jellium model assumed that the more electronegative (usually X-type) ligands bonded to the Au_{13} core might lead to the reduction of potential volume for the confinement of Au_{13} core valence electrons, and result in the destabilization of the superatomic 1P orbitals.[15] In this work, the L-type two-electron-donor pnictine ligands are more suitable to be classified by overall electron-donating ability. $AsPh_3$ is a stronger σ-donating and also a better π-accepting ligand than $SbPh_3$;[59] it is thus envisioned that both interactions may influence the superatomic cluster orbitals. The π-back donation from the Au core to the π-acid ligand is not uncommon, for instance, Au(5d) → CO(π*) in the carbonyl-protected Au cluster,[60] and Au(5d) → N=C(π*) in the guanine-protected Au_{13} cluster.[61]

To get more insight into this, the natural bond orbital (NBO) analyses were performed. The qualitative natural population analyses (NPA) show that the Au_{13} core in **$Au_{13}As_8$** is less negatively charged than that in **$Au_{13}Sb_8$** (−0.50 *vs.* −1.43, Table S9†), as is also the case with the Mulliken charge analysis (−1.95 *vs.* −2.27, Table S10†). This implies that, given the stronger σ-donating ability of $AsPh_3$, a stronger electron back donation from the Au_{13} core to $AsPh_3$ may contribute to the relatively lower electron density for the Au_{13} core in the case of **$Au_{13}As_8$**. As expected, the second-order perturbation theory analyses in NBO basis for **$Au_{13}As_8$** show strong interactions between the central Au lone pair orbitals and the radial Au–As σ* orbitals, as reflected by the large second-order perturbation stabilization energies $E(2)$ (Table S11†). In comparison, this type of interaction in **$Au_{13}Sb_8$** is much weaker (Table S12†). This is probably associated with the fact that the As 4sp orbitals involved in the Au–As σ* orbitals are less diffuse, lower in energy, and thus more electrophilic, compared to the Sb 5sp orbitals in Au–Sb σ* orbitals. Since the stronger π-back donation interactions between Au and Au–As σ* orbitals would reduce the Au–As bond orders more significantly, the Wiberg bond indices for the Au–As bonds in **$Au_{13}As_8$** are indeed smaller (*ca.* 0.46) than those for the Au–Sb bonds in **$Au_{13}Sb_8$** (*ca.* 0.54), whereas those for the innocent Au–Cl bonds in both are almost the same (*ca.* 0.42) (Table S13†). In addition, other types of π-back donation interactions between surface Au lone pairs and As/Sb–C σ* orbitals are rather weak and comparable for both **$Au_{13}As_8$** and **$Au_{13}Sb_8$** (Tables S11 and S12†). Based on these, the upshift of 1P orbitals in **$Au_{13}As_8$** relative to that in **$Au_{13}Sb_8$** is tentatively accounted for by the stronger π-back donation interactions between central Au and radial Au–As σ* orbitals, by which the better π-accepting L-type ligand $AsPh_3$ exerts a similar impact on the Au_{13} core valence electrons to that for the case of the more electronegative X-type ligand.

On the other hand, the correlations of 1D orbitals with the electronegativity of ligands are rather complicated, though they shift to the same direction as 1P orbitals in most cases but lack an obvious trend in the shift amount.[15] In this work, the 1D orbitals in **$Au_{13}As_8$** up-shifted more (by 0.156 eV on average) than 1P orbitals (by 0.031 eV on average). That is to say, the 1D orbitals are more susceptible to the electronic factors of the pnictine ligands. In view of this, more comparative studies, including with the lighter phosphine-protected analogue clusters, may be of interest to better explain the behavior of 1D orbitals with respect to the integrated σ-donating/π-accepting parameters of the L-type pnictine ligands.

Optical properties

The solution photoluminescence (PL) of **$Au_{13}As_8$** emits at *ca.* 802 nm, which is red-shifted in wavelength and also higher in

Open Access Article. Published on 29 May 2023. Downloaded on 2/15/2026 12:58:01 AM. This article is licensed under a Creative Commons Attribution-NonCommercial 3.0 Unported Licence.

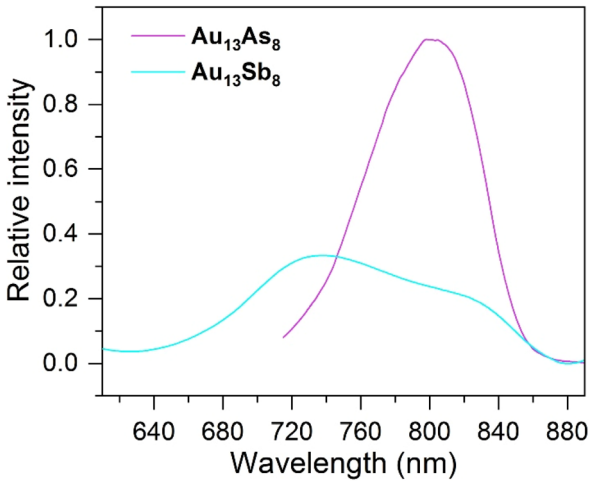

Fig. 5 Photoluminescence spectra for $Au_{13}As_8$ (magenta line, λ_{ex} = 460 nm) and $Au_{13}Sb_8$ (cyan line, λ_{ex} = 470 nm) in CH_2Cl_2 (*ca.* 2.0 mg mL^{-1}) at room temperature.

intensity, as compared to the main emission of **$Au_{13}Sb_8$** at *ca.* 740 nm (Fig. 5). This is presumably due to the heavy metal effect of Sb, which facilitates the reverse intersystem crossing (RISC) process from the T_1 state to the S_1 state and therefore leads to the blue-shift and lower intensity of the emission for **$Au_{13}Sb_8$**.[62,63] The previously reported two phosphine-protected clusters $[Au_{13}(L^P)_nCl_4]^+$ (L^P = trioctylphosphine ($POct_3$), n = 8; L^P = $Ph_2P(CH_2)_3PPh_2$, n = 4) both emit at *ca.* 775 nm.[7] Considering the likely dual emissions of **$Au_{13}Sb_8$**, if the shoulder at *ca.* 825 nm is of the same phosphorescence character as the emissions of **$Au_{13}As_8$** and $[Au_{13}(L^P)_nCl_4]^+$, the emission wavelengths would be in the order of **$Au_{13}Sb_8$** > **$Au_{13}As_8$** > $[Au_{13}(L^P)_nCl_4]^+$.

$Au_{13}As_8$ in its crystalline state exhibits a PL emission over a wider range of wavelengths (from *ca.* 650 nm to *ca.* 850 nm), and the emission maximum at *ca.* 740 nm is blue-shifted by *ca.* 60 nm compared to that in solution. The PL emission of **$Au_{13}Sb_8$** in the crystalline state displays a similar but also blue-shifted weak dual-emission-like pattern to that in solution, with an emission peak centered at *ca.* 805 nm and a shoulder at *ca.* 710 nm (Fig. S10†). In general, the PL blue-shift for both can be partially attributed to the rigidity enhancement of the structures in the solid state. In addition, the largely broadened and blue-shifted solid PL spectrum of **$Au_{13}As_8$**, somewhat resembling that of **$Au_{13}Sb_8$**, also suggest that a similar dual-emission phenomenon to that of **$Au_{13}Sb_8$** may be present in its solid/crystalline state.

Thermal stability

The **$Au_{13}As_8$** is rather stable in the solid state, but gradually decomposes with time in solution at room temperature, although such a process is much slower than for the case of **$Au_{13}Sb_8$**. Lower temperature could effectively inhibit the decomposition of **$Au_{13}As_8$**; its UV-vis monitoring spectra showed no essential decomposition even after 12 days when its DCM solution was stored at 4 °C (Fig. S11†). Thermogravimetric analysis (TGA) of **$Au_{13}As_8$** at a heating rate of 10 °C min^{-1} under N_2 purge (60 mL min^{-1}) showed that the rapid weight loss started at *ca.* 200 °C, whereas that for **$Au_{13}Sb_8$** was observed at 155 °C (Fig. S12†).[39] These results suggest that **$Au_{13}As_8$** is more stable than **$Au_{13}Sb_8$** either in solution or in the solid state but most probably still less stable than the phosphine-protected analogue clusters; this is believed to result from the moderate Au–As bond strength.

Surface reactivity-catalysis

Since the electron-rich Au_{13} core was speculated to activate the C=O bond,[36,64,65] the pnictine-protected Au_{13} clusters may find uses in the aldehyde/ketone-involved catalytic reactions. **$Au_{13}Sb_8$** was found to be able to efficiently catalyze the aldehyde–alkyne–amine (A^3) coupling reaction, but the drawback of lower catalytic stability could also not be neglected.[40] To better realize the trade-off between stability and activity, the catalytic performance of **$Au_{13}As_8$** towards the same A^3 coupling reaction was tested (Table 1). It was found that, despite its relatively stronger Au–As coordination bonds, **$Au_{13}As_8$** could also achieve a comparable conversion ratio to **$Au_{13}Sb_8$** after 12 h, probably associated with different reaction kinetics. More importantly, **$Au_{13}As_8$** is catalytically more stable than **$Au_{13}Sb_8$**; it can be simply recovered (and also purified) from the reaction mixture by precipitation with hexane (Fig. S13†), and can be reused for five cycles with only slight decrease in catalytic activity (Fig. S14 and S15†). This finding further underlines the important role of ligands in tuning the catalytic performance and may provide some implications for the design of more practically useful ligand-protected metal nanocluster catalysts.

Surface reactivity-ligand exchange

The exquisite "cluster-to-cluster" synthetic strategy based on ligand exchange has recently become increasingly prevailing.[47,66,67] Taking Au_{13} clusters as examples, reactivity studies on **$Au_{13}Sb_8$** or its bromo-analogue $[Au_{13}(SbPh_3)_8Br_4]^+$ had shown

Table 1 A^3 coupling reactions catalyzed by $Au_{13}As_8$ or $Au_{13}Sb_8$[a]

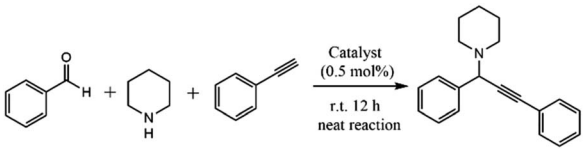

	NMR yield (%)				
Catalyst[b]	Cycle 1	Cycle 2	Cycle 3	Cycle 4	Cycle 5
$Au_{13}As_8$	73	74	69	64	62
$Au_{13}Sb_8$[c]	81	32	—	—	—

[a] Benzaldehyde (1.0 mmol), piperidine (1.2 mmol), phenylacetylene (1.3 mmol), solvent-free reaction. [b] With respect to the amount of benzaldehyde. [c] Given the obvious decomposition in each cycle for **$Au_{13}Sb_8$**, no further trial was made after the second cycle due to the marked decrease in yield.

© 2023 The Author(s). Published by the Royal Society of Chemistry

Open Access Article. Published on 29 May 2023. Downloaded on 2/15/2026 12:58:01 AM.
This article is licensed under a Creative Commons Attribution-NonCommercial 3.0 Unported Licence.

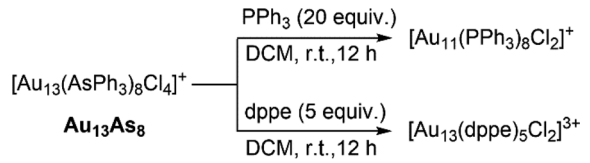

Scheme 2 Reactions of $Au_{13}As_8$ with phosphines.

that they could readily react with glutathione (GSH) or 1-adamantanethiol (S-Adm) to give the achiral $Au_{25}(SG)_{18}$ or chiral $Au_{18}(SAdm)_8(SbPh_3)_4Br_2$, respectively.[39,41] The Wang group also developed a new method of synthesizing thiol-protected Au_{25} clusters through reactions of $[Au_{13}(L'')_8Cl_4]^+$ ($L'' = P(CH_2CH_2CO_2CH_3)_3$) with appropriate thiols.[16] In analogy to these stibine or phosphine-protected Au_{13} clusters, $\mathbf{Au_{13}As_8}$ may also possess the potential as a precursor cluster in the syntheses of other new clusters by reacting with stronger coordinating ligands. Thus, the reactions of $\mathbf{Au_{13}As_8}$ with monophosphine PPh_3 or diphosphine $Ph_2P(CH_2)_2PPh_2$ (dppe) at room temperature were carried out as a proof-of-concept in this work. As shown in Scheme 2, two well-known clusters $[Au_{11}(PPh_3)_8Cl_2]^+$ and $[Au_{13}(dppe)_5Cl_2]^{3+}$ were obtained in the cases of PPh_3 and dppe, respectively, and their structures were determined by comparison of their UV-vis, ^1H NMR and MS spectra with those from literature (Fig. S16–S20†).[7,68] These preliminary trials confirm the potential use of $\mathbf{Au_{13}As_8}$ in the "cluster-to-cluster" syntheses. In comparison, the reactions with $\mathbf{Au_{13}As_8}$ proceed more slowly than with $\mathbf{Au_{13}Sb_8}$, indicating that it is more likely for the former to realize more controlled derivatization or functionalization by ligand engineering.

Conclusions

In this work, a monoarsine-protected icosahedral cluster $[Au_{13}(AsPh_3)_8Cl_4]^+$ ($\mathbf{Au_{13}As_8}$) was prepared. It is isostructural with its previously reported stibine analogue $[Au_{13}(SbPh_3)_8Cl_4]^+$ ($\mathbf{Au_{13}Sb_8}$), which provides an opportunity to better comparatively study the heavier pnictine ligand effect on their electronic structures, optical properties, and surface reactivities. The influencing mechanism of the L-type pnictine ligands on the Au_{13} superatomic orbitals may be different from those of the X-type ligands (*e.g.*, organic thiol, selenol, alkynyl). The superatomic 1P and 1D orbitals of $\mathbf{Au_{13}As_8}$ are up-shifted relative to those of $\mathbf{Au_{13}As_8}$, which is tentatively ascribed to the stronger π-back donation interactions between the Au_{13} core and $AsPh_3$ ligands. In addition, compared to the thermodynamically less stable $\mathbf{Au_{13}Sb_8}$, a better trade-off between stability and activity was realized with $\mathbf{Au_{13}As_8}$, as reflected by its good catalytic performance towards the A^3 coupling reaction. Finally, the ligand exchange reactions between $\mathbf{Au_{13}As_8}$ with phosphines, as exemplified by PPh_3 and $Ph_2P(CH_2)_2PPh_2$, suggest that $\mathbf{Au_{13}As_8}$ may be a good precursor cluster and may find more use in the preparation of other clusters *via* the prevailing "cluster-to-cluster" strategy. Taken together, the heavier organometalloidal arsines or organometallic stibines, especially the latter, are not simply "weaker organic phosphines", and they are more likely to exert distinct ligand effects on the structures and properties of metal nanoclusters. Since there has been only a limited number of heavier pnictine-protected metal nanoclusters, more diverse syntheses of such type of clusters, as well as explorations of their physicochemical properties and applications, are of much interest and deserve deeper scrutiny.

Data availability

All experimental and computational data associated with this article have been included in the main text and ESI.†

Author contributions

Y.-Z. L. and D. S. conceived the manuscript; J. H. Y. performed the experiments; J.-H. Y., Z.-R. Y., J. X., J.-G. W., M. A., T.-D. L. and Y.-Z. L. analyzed data, prepared figures and provided conceptual contributions; J. H. Y., Y. Z. L. and D. S. wrote the manuscript with contributions from all co-authors.

Conflicts of interest

There are no conflicts to declare.

Acknowledgements

We gratefully acknowledge the financial support from the Natural Science Foundation of China (no. 22001139, 22178184, and 52072190), Natural Science Foundation of Shandong Province (no. ZR2022MB099), the Taishan Scholar Project of Shandong Province of China (no. tsqn201812003 and ts20190908), the Fok Ying Tong Education Foundation (171009), the National Postdoctoral Innovative Talents Support Program (No. BX2021171), the China Postdoctoral Science Foundation (No. 2021M700081), and the Science, Education and Industry Integration Pilot Project Program from Qilu University of Technology (Shandong Academy of Science) (no. 2022PY066 and 2022JBZ02-04). Dr M. Azam also acknowledges the financial support through the Researchers Supporting Project (RSP2023R147) at King Saud University, Riyadh, Saudi Arabia.

Notes and references

1 M. McPartlin, R. Mason and L. Malatesta, *J. Chem. Soc. D*, 1969, 334.
2 C. E. Briant, B. R. C. Theobald, J. W. White, L. K. Bell, D. M. P. Mingos and A. J. Welch, *J. Chem. Soc., Chem. Commun.*, 1981, 201–202.
3 R. C. B. Copley and D. M. P. Mingos, *J. Chem. Soc., Dalton Trans.*, 1996, 491–500.
4 J. Akola, M. Walter, R. L. Whetten, H. Häkkinen and H. Grönbeck, *J. Am. Chem. Soc.*, 2008, **130**, 3756–3757.
5 H. Qian, W. T. Eckenhoff, Y. Zhu, T. Pintauer and R. Jin, *J. Am. Chem. Soc.*, 2010, **132**, 8280–8281.
6 Y. Shichibu and K. Konishi, *Small*, 2010, **6**, 1216–1220.

Open Access Article. Published on 29 May 2023. Downloaded on 2/15/2026 12:58:01 AM. This article is licensed under a Creative Commons Attribution-NonCommercial 3.0 Unported Licence.

7 Y. Shichibu, K. Suzuki and K. Konishi, *Nanoscale*, 2012, **4**, 4125–4129.
8 J.-i. Nishigaki, S. Yamazoe, S. Kohara, A. Fujiwara, W. Kurashige, Y. Negishi and T. Tsukuda, *Chem. Commun.*, 2014, **50**, 839–841.
9 X. K. Wan, Q. Tang, S. F. Yuan, D. E. Jiang and Q. M. Wang, *J. Am. Chem. Soc.*, 2015, **137**, 652–655.
10 C. Zeng, Y. Chen, K. Kirschbaum, K. Appavoo, M. Y. Sfeir and R. Jin, *Sci. Adv.*, 2015, **1**, e1500045.
11 R. Jin, C. Liu, S. Zhao, A. Das, H. Xing, C. Gayathri, Y. Xing, N. L. Rosi, R. R. Gil and R. Jin, *ACS Nano*, 2015, **9**, 8530–8536.
12 Y. Song, F. Fu, J. Zhang, J. Chai, X. Kang, P. Li, S. Li, H. Zhou and M. Zhu, *Angew. Chem., Int. Ed.*, 2015, **54**, 8430–8434.
13 L. Liao, S. Zhuang, C. Yao, N. Yan, J. Chen, C. Wang, N. Xia, X. Liu, M. B. Li, L. Li, X. Bao and Z. Wu, *J. Am. Chem. Soc.*, 2016, **138**, 10425–10428.
14 K. Weerawardene, P. Pandeya, M. Zhou, Y. Chen, R. Jin and C. M. Aikens, *J. Am. Chem. Soc.*, 2019, **141**, 18715–18726.
15 S. Takano and T. Tsukuda, *J. Am. Chem. Soc.*, 2021, **143**, 1683–1698.
16 Z. Lei, J. J. Li, Z. A. Nan, Z. G. Jiang and Q. M. Wang, *Angew. Chem., Int. Ed.*, 2021, **60**, 14415–14419.
17 T. Wang, W.-H. Zhang, S.-F. Yuan, Z.-J. Guan and Q.-M. Wang, *Chem. Commun.*, 2018, **54**, 10367–10370.
18 M. Zhou, R. Jin, M. Y. Sfeir, Y. Chen, Y. Song and R. Jin, *Proc. Natl. Acad. Sci. U. S. A.*, 2017, **114**, E4697–E4705.
19 K. Nobusada and T. Iwasa, *J. Phys. Chem. C*, 2007, **111**, 14279–14282.
20 D.-e. Jiang, K. Nobusada, W. Luo and R. L. Whetten, *ACS Nano*, 2009, **3**, 2351–2357.
21 C. Xu, Y. Zhou, J. Yi, D. Li, L. Shi and L. Cheng, *J. Phys. Chem. Lett.*, 2022, **13**, 1931–1939.
22 S. Jin, W. Du, S. Wang, X. Kang, M. Chen, D. Hu, S. Chen, X. Zou, G. Sun and M. Zhu, *Inorg. Chem.*, 2017, **56**, 11151–11159.
23 S. Zhang, L. Feng, R. Senanayake, C. M. Aikens, X.-P. Wang, Q. Zhao, C.-H. Tung and D. Sun, *Chem. Sci.*, 2018, **9**, 1251–1258.
24 L. Yang, H. Cheng, Y. Jiang, T. Huang, J. Bao, Z. Sun, Z. Jiang, J. Ma, F. Sun, Q. Liu, T. Yao, H. Deng, S. Wang, M. Zhu and S. Wei, *Nanoscale*, 2015, **7**, 14452–14459.
25 L. Yang, L. Huang, X. Song, W. He, Y. Jiang, Z. Sun and S. Wei, *Acta Phys.-Chim. Sin.*, 2018, **34**, 762–769.
26 Y. Lv, X. Kang, S. Yang, T. Chen, A. Liu, H. Yu and M. Zhu, *RSC Adv.*, 2017, **7**, 51538–51545.
27 H. Hirai, S. Takano, T. Nakamura and T. Tsukuda, *Inorg. Chem.*, 2020, **59**, 17889–17895.
28 N. Fedik, A. I. Boldyrev and A. Munoz-Castro, *Phys. Chem. Chem. Phys.*, 2019, **21**, 25215–25219.
29 J. Wei, P. L. Rodriguez-Kessler, J. F. Halet, S. Kahlal, J. Y. Saillard and A. Munoz-Castro, *Inorg. Chem.*, 2021, **60**, 8173–8180.
30 S. Takano, H. Hirai, T. Nakashima, T. Iwasa, T. Taketsugu and T. Tsukuda, *J. Am. Chem. Soc.*, 2021, **143**, 10560–10564.
31 Y. Yang, Q. Zhang, Z.-J. Guan, Z.-A. Nan, J.-Q. Wang, T. Jia and W.-W. Zhan, *Inorg. Chem.*, 2019, **58**, 3670–3675.
32 Y. Shichibu, Y. Ogawa, M. Sugiuchi and K. Konishi, *Nanoscale Adv.*, 2021, **3**, 1005–1011.
33 H. Hirai, T. Nakashima, S. Takano, Y. Shichibu, K. Konishi, T. Kawai and T. Tsukuda, *J. Mater. Chem. C*, 2023, **11**, 3095–3100.
34 J. Zhang, Y. Zhou, K. Zheng, H. Abroshan, D. R. Kauffman, J. Sun and G. Li, *Nano Res.*, 2018, **11**, 5787–5798.
35 Z. Wei, W. Jiang, Z. Bai, Z. Lian, Z. Wang and F. Song, *Eur. Phys. J. D*, 2017, **71**, 237.
36 J.-Q. Fan, Y. Yang, C.-B. Tao and M.-B. Li, *Angew. Chem., Int. Ed.*, 2023, **62**, e202215741.
37 S. Zhuang, D. Chen, W.-P. Ng, D. Liu, L.-J. Liu, M.-Y. Sun, T. Nawaz, X. Wu, Y. Zhang, Z. Li, Y.-L. Huang, J. Yang, J. Yang and J. He, *JACS Au*, 2022, **2**, 2617–2626.
38 Y. Shichibu, F. Zhang, Y. Chen, M. Konishi, S. Tanaka, H. Imoto, K. Naka and K. Konishi, *J. Chem. Phys.*, 2021, **155**, 054301.
39 Y.-Z. Li, R. Ganguly, K. Y. Hong, Y. Li, M. E. Tessensohn, R. Webster and W. K. Leong, *Chem. Sci.*, 2018, **9**, 8723–8730.
40 Y.-Z. Li and W. K. Leong, *RSC Adv.*, 2019, **9**, 5475–5479.
41 J. B. Patty, S. Havenridge, D. Tietje-Mckinney, M. A. Siegler, K. K. Singh, R. Hajy Hosseini, M. Ghabin, C. M. Aikens and A. Das, *J. Am. Chem. Soc.*, 2022, **144**, 478–484.
42 Q. Tang and D.-e. Jiang, *Chem. Mater.*, 2017, **29**, 6908–6915.
43 A. Muñoz-Castro, *Inorg. Chem. Front.*, 2019, **6**, 2349–2358.
44 M. R. Narouz, S. Takano, P. A. Lummis, T. I. Levchenko, A. Nazemi, S. Kaappa, S. Malola, G. Yousefalizadeh, L. A. Calhoun, K. G. Stamplecoskie, H. Häkkinen, T. Tsukuda and C. M. Crudden, *J. Am. Chem. Soc.*, 2019, **141**, 14997–15002.
45 H. Shen, S. Xiang, Z. Xu, C. Liu, X. Li, C. Sun, S. Lin, B. K. Teo and N. Zheng, *Nano Res.*, 2020, **13**, 1908–1911.
46 H. Yi, K. M. Osten, T. I. Levchenko, A. J. Veinot, Y. Aramaki, T. Ooi, M. Nambo and C. M. Crudden, *Chem. Sci.*, 2021, **12**, 10436–10440.
47 M. Bevilacqua, M. Roverso, S. Bogialli, C. Graiff and A. Biffis, *Inorg. Chem.*, 2023, **62**, 1383–1393.
48 A. Wing-Bocanegra and A. Tlahuice-Flores, *Phys. Chem. Chem. Phys.*, 2019, **21**, 23855–23864.
49 Z.-H. Gao, J. Dong, Q.-F. Zhang and L.-S. Wang, *Nanoscale Adv.*, 2020, **2**, 4902–4907.
50 P. L. Rodríguez-Kessler, M. Rojas-Poblete and A. Muñoz-Castro, *Phys. Chem. Chem. Phys.*, 2021, **23**, 18035–18043.
51 A. Munoz-Castro, *Phys. Chem. Chem. Phys.*, 2022, **24**, 17233–17241.
52 J. Wei, S. Kahlal, J. F. Halet, J. Y. Saillard and A. Munoz-Castro, *J. Phys. Chem. A*, 2022, **126**, 536–545.
53 G. E. Johnson, A. Olivares, D. Hill and J. Laskin, *Phys. Chem. Chem. Phys.*, 2015, **17**, 14636–14646.
54 G. Shafai, S. Hong, M. Bertino and T. S. Rahman, *J. Phys. Chem. C*, 2009, **113**, 12072–12078.
55 M. Richter and J. Strähle, *Z. Anorg. Allg. Chem.*, 2001, **627**, 918–920.
56 B. S. Gutrath, U. Englert, Y. Wang and U. Simon, *Eur. J. Inorg. Chem.*, 2013, **2013**, 2002–2006.
57 S. Mukherjee, A. Das, A. K. Das, A. Sheriff, K. Sunny, A. S. Nair, S. Bhandary, R. Bhowal, D. Chopra, B. Pathak,

© 2023 The Author(s). Published by the Royal Society of Chemistry

Open Access Article. Published on 29 May 2023. Downloaded on 2/15/2026 12:58:01 AM.
This article is licensed under a Creative Commons Attribution-NonCommercial 3.0 Unported Licence.

S. Yamazoe and S. Mandal, *Chem. Mater.*, 2023, **35**, 1659–1666.
58 I. Tuvi-Arad, G. Alon and D. Avnir, *CoSyM*, **http://csm.ouproj.org.il**.
59 N. J. Holmes, W. Levason and M. Webster, *J. Chem. Soc., Dalton Trans.*, 1998, 3457–3462.
60 A. Fielicke, G. von Helden, G. Meijer, D. B. Pedersen, B. Simard and D. M. Rayner, *J. Am. Chem. Soc.*, 2005, **127**, 8416–8423.
61 X. Zhang, C. Q. Sun and H. Hirao, *Phys. Chem. Chem. Phys.*, 2013, **15**, 19284–19292.
62 X. Cao, K. Pan, J. Miao, X. Lv, Z. Huang, F. Ni, X. Yin, Y. Wei and C. Yang, *J. Am. Chem. Soc.*, 2022, **144**, 22976–22984.
63 X. Jiang, T. Zhang, C. Sun, Y. Meng and L. Xiao, *Chin. Chem. Lett.*, 2019, **30**, 1055–1058.
64 Y. Zhu, H. Qian, B. A. Drake and R. Jin, *Angew. Chem., Int. Ed.*, 2010, **49**, 1295–1298.
65 Y. Pei, N. Shao, Y. Gao and X. C. Zeng, *ACS Nano*, 2010, **4**, 2009–2020.
66 Y. Shichibu, Y. Negishi, T. Tsukuda and T. Teranishi, *J. Am. Chem. Soc.*, 2005, **127**, 13464–13465.
67 W. Suzuki, R. Takahata, Y. Chiga, S. Kikkawa, S. Yamazoe, Y. Mizuhata, N. Tokitoh and T. Teranishi, *J. Am. Chem. Soc.*, 2022, **144**, 12310–12320.
68 L. C. McKenzie, T. O. Zaikova and J. E. Hutchison, *J. Am. Chem. Soc.*, 2014, **136**, 13426–13435.

© 2023 The Author(s). Published by the Royal Society of Chemistry